

# Comparative Performance Analysis of Spectral Estimation Algorithms and Computational Optimization of a Multispectral Imaging System for Print Inspection

Eva M. Valero,<sup>1\*</sup> Yu Hu,<sup>1</sup> Javier Hernández-Andrés,<sup>1</sup> Timo Eckhard,<sup>1</sup> Juan L. Nieves,<sup>1</sup> Javier Romero,<sup>1</sup> Markus Schnitzlein,<sup>2</sup> Dietmar Nowack<sup>2</sup>

<sup>1</sup> Department of Optics, Faculty of Sciences, University of Granada, Campus Fuentenueva, s/n 18071 Granada, Spain

<sup>2</sup> Chromasens GmbH, Max-Stromeier-Strasse 116, 78467 Konstanz, Germany

Received 14 December 2011; revised 4 May 2012; accepted 7 June 2012

*Abstract:* We have analyzed the performance of simulated multispectral systems for the spectral recovery of reflectance of printer inks from camera responses, including noise. To estimate reflectance we compared the performance of four algorithms which were not comparatively tested using the same data sets before. The criteria for selection of the algorithms were robustness against noise, amount of data needed as inputs (training set, spectral responsivities) and lacking of use of dimensionality reduction techniques. Three different sensor sets and training sets were used. We analyzed the differences in the spanning of the subspaces found for the three training sets, concluding that the ink reflectances have characteristic features. The best performance was obtained using the kernel and the radial basis function neural-net-based algorithms for the training set composed of printer inks reflectances, whereas for the other two training sets (composed of samples from the ColorChecker DC and Vhrel's reflectances' set) the quality of the recovered samples was more uniform among the algorithms. We also have per-

formed an optimization to choose the best sensor set for the multispectral system with a reduced number of sensors. © 2012 Wiley Periodicals, Inc. *Col Res Appl*, 39, 16–27, 2014; Published online 31 July 2012 in Wiley Online Library (wileyonlinelibrary.com). DOI 10.1002/col.21763

*Key words:* multispectral imaging; spectral estimation

## INTRODUCTION

The usefulness of having access to the spectral information of an image on a pixel-by-pixel basis is well known in a wide range of different applications.<sup>1</sup> In recent years spectral imaging has been a quite active field of research. The problem of obtaining spectral reflectances or radiances with enough spatial accuracy can be tackled essentially by two different approaches: the most immediate approach is possibly the design of a capture device that works with a high number of spectral bands and provides the spectral data directly with a reasonable sampling interval in wavelength, as in ultra and hyperspectral systems (more than 30 spectral bands, using narrow-band filters, tunable filters, or diffractive devices coupled to a monochrome imaging sensor<sup>2</sup>); a less straightforward and less accurate but also less expensive and easier to implement strategy is to obtain an estimation of the spectral information from a reduced number of sensor responses (color camera plus one or two color filters) using a suitable estimation algorithm, as in multispectral systems.<sup>3</sup>

\*Correspondence to: Eva M. Valero (e-mail: valerob@ugr.es).

Contract grant sponsor: Chromasens GmbH in the Color Imaging Lab (University of Granada); contract grant number: REF. 3420-00.

Contract grant sponsor: Regional government (Junta de Andalucía); contract grant number: P07-TIC-02642.

Spectral estimation from sensor responses in the multispectral approach is a typical example of an ill-posed problem, as the number of sensor responses (usually from 3 to 9) is always lower than the number of spectral bands which are estimated.

In the last 20 years, several spectral estimation algorithms have been proposed for dealing with this problem, some based on real sensor responses and some on computational simulations of sensor responses.<sup>4–10</sup> Most of them have been tested including the addition of noise to the sensor responses to mimic the behavior of real capture devices.

Such multispectral capture systems have been tested in several applications, from artworks study and reproduction<sup>11</sup> to food quality inspection,<sup>12</sup> and there are new potential fields of use for these technologies continuously arising.<sup>13</sup> Among them, there is the field of spectral printing<sup>14</sup> and spectral characterization of printing devices for color correction or color quality assessment of printed samples.

The basic working tools for spectral printing applications are the reflectances of the printer ink samples. For industrial printing applications it is particularly interesting to use devices that can measure various samples, spatially distributed over the substrate, simultaneously and accurately. The printing industry demands fast, simple, and accurate color quality evaluation of the printing process. Usually, print inspection is performed either visually or using a spectrophotometer or colorimeter to measure the color of the printed samples and compare it with a reference. The quantified difference is aimed to be less than a defined threshold, commonly based on a minimum perceptible color difference. It is obvious that this field offers potential applications for multispectral capture devices. This is especially true when we take into account that for many printing companies the use of hyperspectral systems would be unattainable for reasons of economy and speed. None of the previous studies in the multispectral field, to our knowledge, tackles the design of a suitable multispectral capture system for the spectral estimation of printer inks, although in Ref. 15 some printed samples are used for the estimation of spectra from tristimulus values. Multispectral capture systems used specifically for inline colorimetric quality control of printed samples on paper offer the advantages of allowing simultaneous measurements of many samples using a relatively simple and economic device. The subspaces spanned by the set of printer ink reflectances are different from those spanned by other widely used collections of samples, as we will show in the next section.

The main aim of our work is to study the influence of several factors on the estimation quality of printer inks reflectances such as: the inclusion of noise in the camera responses, training set selection, type of estimation algorithm, and finally the optimum sensor selection for the task. We do not intend to tackle the task of sensor design for ink reflectance estimation, but rather test which sensor set among several representative ones would perform

better. We have simulated additive noise in the camera responses, and compared the performance of the spectral estimation algorithms for noise-free and noisy camera responses. We used three different training sets, one composed of ink reflectances (specific for our task, although not specifically optimized for spectral estimation) and the other two of widely used reflectance sets in the field of spectral estimation. Using these reflectance data and some dimensionality reduction techniques, we have been able to prove that ink reflectance spectra are not well reproduced using other reflectance sets' basis functions. We selected four state of the art spectral estimation algorithms: pseudoinverse,<sup>6</sup> kernel,<sup>10</sup> projection onto convex sets (POCS),<sup>16</sup> and radial-basis-function neural network (RBFNN),<sup>17</sup> and also introduced some additional constraints and modifications from the original proposals, described in detail in "Spectral Estimation Algorithms" section. To our knowledge, the performance of these set of algorithms for a highly specific task as ink reflectance spectral estimation has not been previously analyzed comparatively. Finally, we studied the possibility of finding an optimal subset of sensors for ink reflectance estimation to reduce the complexity of the capture device. The results of our computations shed some light on the feasibility of the spectral estimation approach and how it could be optimized. We are convinced that our results could be of use for future practical developments of a multispectral system specifically designed for spectral printing applications and inline print color quality assessment.

## METHODS

### Simulation of Camera Responses and Noise

We have simulated the multispectral capture by using different sensor sets (see "Sensor Sets" section for details of the sensors) according to Eq. (1):

$$r_{i,n_j} = \sum_{\lambda=\lambda_1}^{\lambda_2} S(\lambda)E(\lambda)q_i(\lambda) + n_{i,j} = r_i + n_{i,j} \quad (1)$$

where  $S(\lambda)$  is the spectral reflectance of the sample,  $E(\lambda)$  is the spectral power distribution of the light source used to illuminate it (described in "Light Source and Training Samples" section),  $q_i(\lambda)$  is the spectral response of sensor  $i$  and  $[\lambda_1, \lambda_2]$  is the spectral range covered by the sensor set. We have introduced a global term of additive noise  $n_{i,j}$  in Eq. (1) to model representative noise sources in real capture devices. The modeled noise term includes shot noise and flicker noise, which depend on the magnitude of the camera response. Quantization noise (assuming 10 bits per channel, which is a typical value for a commercial digital camera)<sup>18,19</sup> has been introduced by rescaling and rounding camera responses to the nearest integer in the range [0–1024]. The distribution of noise values covers the shot and flicker noise but not the thermal noise or the dark-current noise, resulting in an estimated averaged SNR of 30 dB, which is a representative value for multi-

spectral image capture devices.<sup>13</sup> Thermal noise and dark current noise are not considered because they are relatively easy to reduce by cooling the camera or performing dark image subtraction. In this study, we are computing camera responses only for spectral estimation purposes. For this specific task, it has been proven that the performance decreases when the overall SNR decreases.<sup>13</sup> The key factor affecting performance is the overall SNR, then, and not the specific type of noise included in it.

We have generated a set of  $j = 100$  different noise values for each  $r_i$  noise-free camera response.<sup>20</sup> These noise values are normally distributed with a standard deviation  $\sigma_i$ , which depends on the noise-free camera response  $r_i$  as described in Eq. (2).

$$\sigma_i = 0.01r_{iw}\sqrt{\frac{r_i}{r_{iw}}} \quad (2)$$

where  $r_{iw}$  is the camera response for sensor  $i$  corresponding to the light source used to illuminate a perfect white. We have found that the parameter 0.01 in Eq. (2) models appropriately the noise behavior of a real capture device.

### Spectral Estimation Algorithms

We have selected four different algorithms which are representative of different strategies for estimating spectral reflectance from few sensor responses. Our selection of algorithms includes the Pseudoinverse,<sup>6</sup> kernel,<sup>10</sup> POCS,<sup>16</sup> and RBFNN.<sup>17</sup> Although POCS has been used to analyze hyperspectral images previously, to the authors knowledge the only instances of previous studies, which describe the way to use it for spectral estimation (specifically, for obtaining metamers of spectra from sensor or visual responses), are Refs. 16 and 21. The well-known Wiener algorithm<sup>8</sup> has also been used widely for spectral estimation, and it has been shown that it can be considered as a particular instance of the more general kernel approach.<sup>10</sup> In a preliminary study<sup>22</sup> using ink reflectances as training set, we found that it did not outperform kernel, RBFNN and POCS and that is why we have not included it for this work.

We have taken the following factors into account in our selection of algorithms.

*Robustness Against Noise.* Most of the selected algorithms have demonstrated some degree of robustness against noise when real camera responses or simulated noisy camera responses were provided as input.<sup>9,10,23</sup> An exception is the pseudoinverse approach which has been shown to decrease performance significantly for noisy data.<sup>24</sup> The RBFNN algorithm is also slightly more sensitive to noise even if it is trained with noisy data, because the introduction of noise interferes with the estimation process by making it more difficult to find the optimal set of weights and appropriate network configuration. The POCS has not been tested previously with noisy camera responses for spectral estimation, so our results will provide some insight in assessing its robustness against noise.

*Amount of Data Needed as Input (e.g., Sensor Spectral Responsivity or Training Set of Reflectances).* The POCS algorithm needs the spectral responsivity of the sensor set as input, which can be a drawback if the capture system is not fully characterized from a spectral point of view (calibration). None of the other algorithms require the spectral responsivity, but all of them except POCS need a set of reflectances for which the sensor responses are known (training set), and so they make use of a priori information. In general, the problem of spectral estimation can be seen as a problem of fitting spectral information using camera responses. Therefore, most of the approaches used in this work need a training set to obtain the optimal fit. From a slightly different perspective, spectral estimation can be seen as a mapping process between camera responses and reflectances or radiances. In fact, algorithms that provide this kind of ad hoc mapping (for instance neural networks<sup>17</sup>) have recently been applied to the problem of spectral estimation as well.<sup>23</sup> The fact that most algorithms need a training set poses the question of adequate sample selection and the influence of the process of building an adequate training set on the spectral estimation quality.<sup>25</sup> Nevertheless, a training set is not always necessary. The POCS approach can be used for spectral estimation by incorporating some positivity and smoothness constraints without any a priori information about reflectances. The smoothness constraint is not included in the original proposal of the POCS algorithm<sup>21</sup>; however, we have introduced it in our implementation as it has shown to improve estimation quality. The POCS algorithm uses as input the spectral responsivity of the sensor sets and tries to find optimal spectra that match the projections of the experimental data (test reflectance samples) onto the sensors, and therefore, are metamers for this sensor set. See ‘‘Detailed description of the implementation’’ section for details on the implementation of each of the algorithms.

*Dimensionality Reduction of the Spectral Data.* Some estimation algorithms use dimensionality reduction techniques for the spectral data, either based on linear models (such as principal component analysis PCA,<sup>26</sup> independent component analysis ICA,<sup>27</sup> non-negative matrix factorization (NMF)<sup>28</sup>], or by introducing some nonlinearities in the standard linear approach.<sup>29</sup> The dimensionality reduction techniques are useful for dealing with the fact that the spectral estimation problem is ill-posed due to the imbalance between the relatively few number of camera responses and the relatively high number of data (bands) needed in the spectral signals. The Imai–Berns,<sup>5</sup> Maloney–Wandell,<sup>4</sup> and Shi–Healey<sup>7</sup> methods are instances of spectral estimation methods which incorporate dimensionality reduction techniques. None of the four selected algorithms in our study incorporates dimensionality reduction techniques, for two main reasons: first, in a preliminary study<sup>22</sup> none of these algorithms was found to offer better estimation performance than the ones selected for this study; and second, we think that to perform the dimensionality reduction properly, some work has to be dedi-

cated to an appropriate selection of samples which are not necessarily included in the training set.

*Detailed Description of the Implementation.* In what follows, we will refer to the set of training camera responses as  $\rho_T$ ; the set of training reflectances will be denoted by  $R_T$ ; the set of training color signals (training reflectances illuminated by the light source described in “Light Source and Training Samples” section) will be  $C_T$ ; the estimated reflectance (only one at a time, as we are using the “leave-one-out” cross validation method,<sup>30</sup> see “Training Set 1 and Full Spectral Range” section for details) will be called  $R$  and the estimated color signal  $C$ . The corresponding camera responses from which the spectral information is estimated will be called  $\rho$ .

### *Pseudoinverse algorithm*<sup>6</sup>

Given a set of training spectra  $C_T$  and the corresponding set of camera responses  $\rho_T$ , a recovery transformation matrix  $D$  is defined by:

$$D = C_T \times \rho_T^{\dagger} \quad (3)$$

where  $\rho_T^{\dagger}$  is the pseudoinverse of  $\rho_T$ . For full rank matrices, the pseudoinverse is defined as:

$$\rho_T^{\dagger} = (\rho_T' \times \rho_T)^{-1} \times \rho_T' \quad (4)$$

where  $\rho_T'$  is the transpose of  $\rho_T$ . An estimate  $C_{pi}$  of a test spectra is obtained from the corresponding camera responses by applying the transformation  $D$ , that is,

$$C_{pi} = D \times \rho \quad (5)$$

For instance, if the number of sensors is 12 and we have 159 spectral signals in the training set, then  $C_T$  is of dimensions  $(81 \times 159)$ , assuming 5 nm sampling with spectral range of the signals from 380 to 780 nm (this will not always be the case, see “Results and Discussion” section for details);  $\rho_T$  is of dimensions  $(12 \times 159)$ ,  $D$  is of dimension  $(81 \times 12)$ , and  $\rho$  is a  $(12 \times 1)$  vector of camera responses. We finally obtain an estimate  $C_{pi}$  of dimension  $(81 \times 1)$ . The reflectances are obtained from the estimated color signals by discounting the illumination. This is a feasible and practical approach for our application related to printed samples, since the illumination will be known for the acquisition of real camera responses. Also, we have found an increase in estimation quality if reflectances are obtained from recovered color signals instead of being estimated directly. The pseudoinverse is a very simple nonparametric algorithm, for which the estimation quality only depends on the training and test data set.

### *Kernel algorithm*<sup>10</sup>

In the kernel algorithm, direct estimation of reflectances leads to a better estimation performance, as compared to estimation of color signals (as proposed for the pseudoinverse approach). In this method, the camera responses are transformed onto a feature space via the kernel function, and in this space ridge regression estimation is performed to obtain the estimated reflectances. Alternatively, the

method can be described as performing a backprojection of camera responses to spectral space, a correlation with the training set and a computation of a set of coefficients to recombine the training set spectra.<sup>10</sup>

The first step is to calculate the Gaussian kernel matrices  $K$  and  $\kappa$ , according to Eqs. (24) and (25) of reference:<sup>10</sup>

$$K_{jm} = \exp\left(-\frac{(C_{Tj} - C_{Tm})' \times W' \times W \times (C_{Tj} - C_{Tm})}{2\sigma^2}\right) \quad (6)$$

where  $C_{Tj}$  and  $C_{Tm}$  are column vectors formed by the color signals corresponding to samples  $j$  and  $m$  of the training set, and  $W$  is a matrix containing the spectral responsivities of the sensors (each column corresponding to a channel responsivity). In case of a real camera system, the kernel method does not require the spectral responsivities as an input. For this work, however,  $W$  is introduced for computing the camera response simulations. The parameter  $\sigma$  is defined as the effective area of the kernel.

The second kernel function, matrix  $\kappa$ , is calculated for each estimated sample  $i$  as:

$$\kappa_j = \exp\left(-\frac{(\rho_j - \rho_i)' \times (\rho_j - \rho_i)}{2\sigma^2}\right) \quad (7)$$

where  $\kappa_j$  represents a column of the matrix  $\kappa$ , and  $j$  is the index of training samples, varying from 1 to 159 in our case. This kernel matrix creates a feature space with the same dimension as the number of samples, according to Ref. 10.

After obtaining the kernel matrices, the estimation for sample  $i$  is calculated as follows:

$$R_k = R_T \times (K + \gamma I)^{-1} \times \kappa' \quad (8)$$

The parameters  $\gamma = 0.001$  and  $\sigma = 75$  were found by brute force optimization to optimize estimation quality.  $\gamma$  is a regularization term introduced in the recovery equation to prevent instabilities in the matrix inversion. The optimal parameters vary much depending on the training set, which makes the algorithm lose generality in comparison with the nonparametric algorithms, although at the same time allows for a better estimation quality, as we will show in “Results and Discussion” section.

### *POCS algorithm*<sup>16</sup>

The POCS algorithm works iteratively by computing normalized projections of the initial estimates onto the responsivities of the sensor set (multiplied by the Spectral Power Distribution (SPD) of the illumination). Further, the initial estimate is corrected in each step by decreasing the difference between the projection and the sensor response, maintaining a positivity constraint. As a final step, the estimate is smoothed to suppress spikes in the estimated spectral reflectances. POCS provides as final output a metamer of the test spectrum for the sensor responsivity set. The algorithm is parametric because the number of iterations influences the performance. We will now describe the computational steps in our implementation of this algorithm.

First, we compute a weighted responsivity matrix by multiplying each sensor responsivity by the SPD of the illumination ( $\mathbf{W}_{\text{SPD}}$ ). We also calculate the square of the Euclidean norm  $N_j$  for each column  $j$  of the matrix  $\mathbf{W}_{\text{SPD}}$ . The algorithm is initialized by the “first estimate” vector  $\mathbf{F}_1$ ; in our case selected as the SPD of the illumination. Then, for each iteration  $n$  and each sensor  $j$ , we compute the ratio  $G_j$  as follows:

$$G_j = \frac{F'_n \times W_{\text{SPD}j} - \rho'_{ij}}{N_j} \cdot W'_{\text{SPD}j} \quad (9)$$

In Eq. (9)  $\rho_{ij}$  is the sensor response corresponding to sample  $i$  for sensor  $j$ . Afterwards, we correct the initial estimate by subtracting  $G_j$  from  $F_n$ . We then introduce the positivity constraint by setting all negative values of the new estimate to zero. Smoothing of the estimate is performed by local averaging. The smoothing post-processing step was not introduced in the original proposal of the algorithm.<sup>16</sup> The algorithm converges iteratively to the best estimate  $R_{\text{POCS}}$  for each sample. It shall be noted, that this algorithm does not need any training data. The quality of estimation, however, depends on the number of iterations used in the algorithm, which we found to be approximately 400 for our data set. We also see possible enhancements in alternative implementations for the smoothing part of the algorithm and alternative candidates for the initial estimate. The optimization of such factors for our particular application will be a matter of future work.

### **RBFNN algorithm<sup>17</sup>**

The underlying idea of this neural networks approach to spectral estimation is to obtain a mapping between camera responses and spectral reflectances, based on a neural network with an appropriate structure and weight distribution of neurons. The RBFNN was implemented using the Matlab Neural Network toolbox with a Gaussian Radial Basis Function. We set the mean square error goal to zero and fixed the spread of the Gaussian function to a rather large number of 40 neurons for our data, aiming in estimation of smooth functions. We allowed the heuristics of the Radial Basis Function to add a maximum number of 30 neurons during the training process. The training process links normalized training camera responses, which are the input of the network, to training normalized reflectances at the output by adapting the neuronal weight vectors to satisfy the specified error goal. The outlined parameters were already found to perform well in a previous work with a restricted set of sensors.<sup>22</sup> The final structure of the network consists of 6–12 neurons in the input layer (the same as the number of sensor responses), 30 neurons in the hidden layer and 52–81 neurons in the output layer (the same as the dimensionality of the spectral signals). As outlined above, the training process is performed for normalized camera responses and normalized reflectances in the range from 0 to 1. The estimation is performed in the same manner for camera responses normalized to the same range as the training data, leading to normalized

estimated reflectances. To obtain reflectances in the original range, the estimated reflectances can be scaled back to the initial range using the normalization parameters of the training. The RBFNN algorithm has the drawbacks of being very sensitive to an adequate selection of the training set (see “Light source and Training samples” section where this factor is discussed using our data) and also of being somewhat computationally demanding, due to the iterative training process. However, once the network is trained, spectral estimation is a very fast process.

### **Sensor Sets**

We have used three different sensor sets to simulate the multispectral system camera responses. The first one (sensor set A) is composed of 12 equidistant gaussian filters with 40 nm FWHM, and equi-spaced peak wavelengths between 370 and 800 nm [Fig. 1(a)]. The two additional sensor sets are composed of the transmittances of real multi-bandpass filters (Optics Balzer AG, Liechtenstein) combined with a typical CCD sensor spectral responsivity. Sensor set B is composed of 12 bandpass filters covering the full spectral range [from 380 to 780 nm, see Fig. 1(b)]. Sensor set C is composed of six bandpass filters with a reduced spectral range between 430 and 685 nm [Fig. 1(c)]. Sensor sets B and C correspond to NEC  $\mu\text{PD8821CZ-A}$ , included in the camera Aleos 7300-60 of Chromasens GmbH, (Germany).

Sensor set A was built with the aim of examining the performance of a group of ideal sensors, while sensor sets B and C correspond to real filters multiplied by a real sensor spectral responsivity and lead to a more realistic model of a capture system. The main difference between sensor sets B and C is the spectral range covered by each set and the number of sensors. Therefore, we will compare the performance of a complex system with a high number of sensors, covering the full spectral range for the visible (sensor set B), with the performance of a reduced number of sensors not covering that range entirely (sensor set C). In addition, we considered selecting an optimal subset of six to eight sensors from sets A and B, leading to an enhanced segmentation quality. The exhaustive search for sensor selection is described in the results section.

### **Light Source and Training Samples**

For the simulation of camera responses of each sensor set [see Eq. (1)] a white LED source with a known spectral power distribution (SPD) was assumed [Fig. 2(a)]. We have selected this light source because it offers sufficient emission in the visible range and because its SPD is much smoother than other alternatives such as fluorescent sources. Previous research has shown that spectral estimation with spiky illumination is more difficult than using illumination sources with smooth spectra.<sup>28</sup> Another advantage of LED over other typical smooth light sources (i.e., incandescent lamps) is the relatively higher emission at short wavelengths. Apart from that, LED illumination

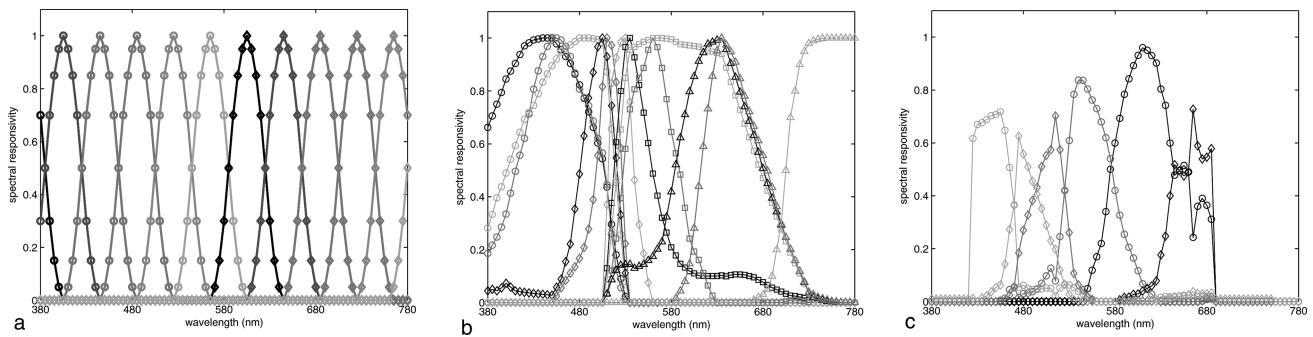


FIG. 1. Spectral responsivity curves of the three sensor sets used. (a) Sensor set A. (b) Sensor set B. (c) Sensor set C.

is a very common source in printer quality-control application devices.

The importance of an adequate training set selection for the spectral estimation performance of most recovery algorithms was pointed out in “Spectral Estimation Algorithms” section (see also Ref. 31). If we want to estimate the spectral reflectances of inks, the best choice would be to include a representative selection of data measured from printed samples in our training set. One way to investigate the influence of the selection of training samples on the performance of each algorithm is to use alternative training sets containing widely used samples (and none of them containing printer inks) to compare the quality of the ink reflectance estimation for different algorithms with a specific training set that contains only data from printer ink samples. Using additional training sets will also be useful to demonstrate the characteristic features of the printed ink reflectance data, although we do not attempt to describe such features in detail. Our aim is to demonstrate that other sets are less optimal for the estimation of printer ink samples.

For our study, we selected three training sets, one composed of ink samples, whereas the other two sets are built from standard collections of reflectances that do not include printed samples.

*Training set 1* is composed of 160 printer ink samples with reflectances measured from 380 to 780 nm with a 5-nm sampling interval using a spectrophotometer (Ocean Optics HR-4000). Forty-two of these samples were obtained using a Flexo printing machine with inks from SunChemical and Hartmann Inc. (UK). The rest of the samples were selected from a standard printing chart of offset inks, known as the HKS chart (Hostmann-Steinberg, K+E und Schmincke, Germany). The entire set covered most of the gamut of existing printer inks, and colors are roughly regularly distributed in the  $a^*b^*$  color plane, as illustrated in Fig. 2(b).

*Training set 2* is composed of 160 randomly selected samples from the Macbeth Color Checker DC (Gretag-Magbeth, X-Rite). This chart is commonly used for digital camera calibration, but also for multispectral imaging.<sup>32,33</sup> It is built by deposition of pigment on a rigid substrate, and the resulting color patches are assumed to represent both natural and man-made objects reflectances.

*Training set 3* is composed of 160 randomly selected samples from Vhrel’s set.<sup>34</sup> This set includes real measurements from natural and artificial objects.

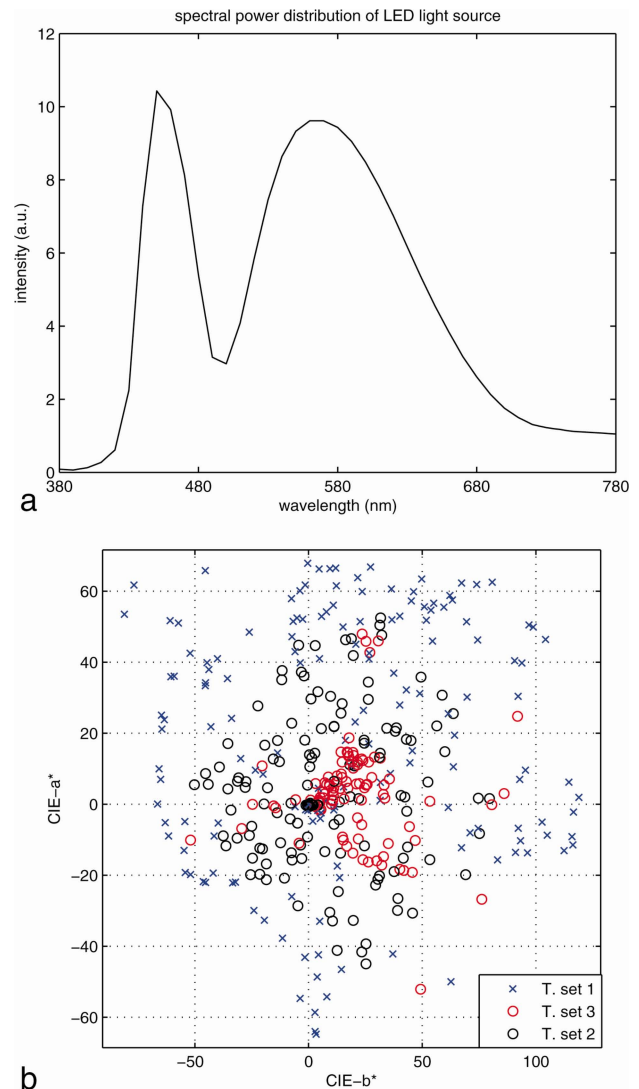


FIG. 2. (a) SPD of the LED light source used in the simulations. (b)  $a^*-b^*$  distribution of values of the three training sets used under the LED light source shown in (a). [Color figure can be viewed in the online issue, which is available at [wileyonlinelibrary.com](http://wileyonlinelibrary.com).]

In Fig. 2(b), we show a plot of the three training sets  $a^*$  and  $b^*$  values calculated using the LED light source represented in Fig. 2(a). We can see that the ink training set covers a wider range of hue values than the other two conventional sets.

We also evaluated the degree of similarity between the training sets using spectral reconstruction performed via three different dimensionality reduction techniques: PCA,<sup>26</sup> ICA,<sup>27</sup> and NMF<sup>28</sup> with five to eight basis vectors. We found that changing the training set for spectral dimensionality reduction results in worse recovery quality for printer inks, and supports the hypothesis that there are differences in the subspaces covered by the basis vectors of the different sets.

We assessed recovery quality using spectral error metrics, because we were interested specifically in differences found between the original and recovered spectral signals. We found a lower recovery quality in goodness-of-fit coefficient (GFC) and root mean square error (RMSE) indices (described in the next section) for training sets 2 and 3 in all cases, when compared to the recovery results obtained using basis vectors of training set 1 (for instance, PCA recovery for eight basis vectors resulted in a GFC of 0.9985 and RMSE 0.014 for training set 1, 0.9957 and 0.0298 for training set 2, and 0.9969 and 0.0257 for training set 3). The quality of recovered samples measured with GFC was found to be better using NMF for dimensionality reduction. If RMSE was used as quality metric, however, ICA performed best. To determine whether these results might be due to the random selection process used in sets 2 and 3, we ran the ICA, NMF, and PCA algorithms on sets 2 and 3 five times and recovered the reflectances of set 1, each time with a different subset of 160 samples (again, randomly selected). Although the quality indices values varied slightly for each run, the trends outlined above for GFC and RMSE were consistent. For all runs, the inks samples offered the best results. Globally, these results show that there is a significant difference in the subspaces spanned by the basis vectors obtained from different training sets. Therefore, the previous results concerning the design of multispectral capture systems, which were obtained using different sets of reflectances, are not strictly valid for the inks set.

### Quality Indices for Spectral Estimation Assessment

We used three metrics to analyze the quality of the spectral estimates obtained by different algorithms. Two of them are based on spectral similarity between the original and estimated samples (the RMSE, and the GFC<sup>35</sup>), and one of them is based on visual perception (the CIE 94 Color difference equation,  $\Delta E_{94}$ , computed using the LED source as reference white and the CIE1931 2 deg standard observer). We chose this color difference equation instead of the more recent and perceptually more accurate CIEDE2000 because it is much simpler to calculate and allows us to perform our comparative analysis of algorithms performance as well. Spectral similarity metrics

and color differences typically show some common trends but not a complete correlation. This shows that it is necessary to include both spectral and colorimetric measures for analyzing spectral estimation results.<sup>36,37</sup> The RMSE index focuses on absolute differences between the original and estimated sample reflectance, and therefore is not independent of scale factors. The GFC quality index is the cosine of the angle formed by the two samples in the high-dimensional vector space of spectral signals. The closer the GFC is to unity, the better the estimation quality of the sample. The GFC is independent of scale factors, so two samples differing only in scale but not in shape would result in a GFC of 1. Both measures are complementary and have different relative importance depending on the kind of spectral recovery (absolute or relative values of reflectance).

## RESULTS AND DISCUSSION

### Training Set 1 and Full Spectral Range

We first present the estimation results obtained for training set 1 (printer inks) in the full spectral range from 380 to 780 nm. In Table I, we show the quality indices corresponding to the four different algorithms and sensor set A. Each quality index distribution is the result of recovering all the samples one by one using the “leave one out” cross validation evaluation method.<sup>30</sup> In other words, for each sample selected for recovery, we use all the remaining samples as a training set (for all the algorithms which require training data). Therefore, the training set changes slightly each time we estimate a different sample. Our main aim was to compare the algorithm performance of the four selected algorithms in the same conditions, and for that we have used three different training sets. For all algorithms except POCS (which does not require training), the estimation results can be compared amongst each other (as they are based on the same training data—training set 1 for results presented in this sub-

TABLE I. Quality indices results for sensor set A, noisy data, different algorithms, and full spectral range for training set 1.

	Kernel	RBF-NN	POCS	Pseudoinv
RMSE				
Mean	<b>0.0025</b>	0.0040	0.0049	0.0046
STD	0.0018	0.0024	0.0030	0.0025
5% p	0.0008	0.0009	0.0010	0.0012
95% p	0.0051	0.0089	0.0104	0.0094
GFC				
Mean	<b>0.9964</b>	0.9946	0.9927	0.9923
STD	0.0080	0.0079	0.0064	0.0093
5% p	0.9997	0.9993	0.9989	0.9989
95% p	0.9875	0.9857	0.9796	0.9727
$\Delta E_{94}$				
Mean	0.8332	1.6715	<b>0.7763</b>	1.0938
STD	0.5165	1.5050	0.5125	1.0902
5% p	0.3048	0.4039	0.2133	0.2242
95% p	1.9165	4.1835	1.8833	2.7139

Best results in bold for each metric.

section). It shall be noted that training set 1 has not been specifically optimized to improve the performance of any of the algorithms. We will leave this issue as a matter for future study.

To recover the full spectral range of the sample does not pose a problem for sensor sets A or B, since these sets cover the entire spectral range. Sensor set C on the other hand covers only a range from 430 to 685 nm and therefore forces a blind estimation for any wavelength outside that range (towards the ends of the spectrum).

We can see from Table I that globally the best results are offered by the kernel algorithm followed by RBFNN according to GFC and RMSE quality measures. In most cases, the average quality of the estimations can be considered acceptable for the specific application of color quality assessment, assuming a threshold of around 1  $\Delta E_{94}$ . The minimum acceptable thresholds for spectral metrics have not been defined for this application, so we can assume the usual values of GFC above 0.99 and RMSE less than 0.025. The POCS algorithm gives the lowest average  $\Delta E_{94}$  color difference and the RBFNN the highest. This can be explained by considering that the aim of the RBFNN is to obtain data as similar as possible to the original reflectances but not necessarily offering a minimal perceptual difference. It therefore does not introduce constraints regarding the location in the spectrum for which differences are allowed to appear between original and recovered data. For some cases such differences might appear in the central portion of the spectrum where they are visually more noticeable. The POCS algorithm offers good colorimetric performance even though it estimates metamers for the camera sensors and not for the human visual system cone responsivities. The worst results in spectral estimation quality correspond to the Pseudoinverse for sensor set A. It shall be noticed that our results cannot be compared directly with other authors' results due to the difference in the sample sets or error metrics used.

Estimation quality for noise-free sensor responses (not shown in Table I) is better than for noisy data, as expected. The biggest difference between noise-free and noisy estimations is found for pseudoinverse (mean GFC of 0.9979, mean RMSE of 0.0024 and mean  $\Delta E_{94}$  of 0.3868 for noise-free data). This shows some potential lack of robustness against noise for this algorithm. In this sense, the kernel method, POCS and RBFNN are found to be relatively less sensitive to noise in the sensor responses.

Apart from the best and worst approaches discussed above, the overall estimation quality is quite similar for all the other algorithms. This shows that we could have a wide range of choice for our particular application, and the final selection for the best algorithm could be dictated by the availability of the inputs needed for a particular solution (such as the spectral responsivity of the sensors or the training data).

When comparing the algorithms' performance for different sensor sets, we found quite similar trends for all evaluated algorithms. In Table II, we present individual results for the three sensor sets, only for the kernel algorithm. The best results for the full spectral range corre-

TABLE II. Quality indices results for the kernel algorithm, different sensor sets and full spectral rangem.

	Sensor set A	Sensor set B	Sensor set C
RMSE			
Mean	<b>0.0025</b>	0.0031	0.0046
STD	0.0018	0.0028	0.0034
5% p	0.0008	0.0010	0.0019
95% p	0.0051	0.0069	0.0113
GFC			
Mean	<b>0.9964</b>	0.9938	0.9827
STD	0.0080	0.0129	0.0479
5% p	0.9997	0.9998	0.9996
95% p	0.9875	0.9728	0.9016
$\Delta E_{94}$			
Mean	<b>0.8332</b>	1.1252	1.2202
STD	0.5165	0.8837	0.7047
5% p	0.3048	0.4309	0.4099
95% p	1.9165	2.2131	2.5533

Best results in bold for each metric.

spond to sensor set A, second best is sensor set B and the worse quality is given by sensor set C. Nevertheless, sensor set A has the disadvantage of not being formed by real sensors. Even if we use a camera coupled with a device producing transmittances similar to Gaussian curves (such as a liquid crystal tunable filter) the combined sensor responsivity would not be Gaussian because it has to be multiplied by the camera sensor responsivity. We get closer to real situations when we evaluate the possibility of using sensor sets B or C.

In Fig. 3, we present some examples of original and recovered reflectances for the RBFNN, Pseudoinverse, POCS, and kernel algorithms for sensor set C. The biggest difference in general between the original and estimated reflectance is found in the extremes of the spectrum (near 380–400 nm or near 730–780 nm). The color matching functions or CMFs, which are needed to calculate the color differences, have negligible values in both ends of the spectrum, so even relatively big discrepancies between original and recovered signals at the beginning and the end of the spectrum do not result in visually perceptible differences. This is one of the reasons why the spectral and colorimetric indices do not always correlate.

If we consider the estimation quality for an application related to human judgment of color differences between samples then we should be less concerned with the discrepancies found in the extremes of the spectral range covered. It seems that in general purple colors are the most difficult samples to estimate. One reason for this is the somewhat spiky nature of the inks in the violet end of the spectrum found in some cases of ink samples. As shown in Fig. 3(a), a purple sample with a smoother reflectance can be estimated very accurately.

### Training Sets 2 and 3 and Reduced Spectral Range

We now discuss the issue of the training set selection. As described in "Light Source and Training Samples"

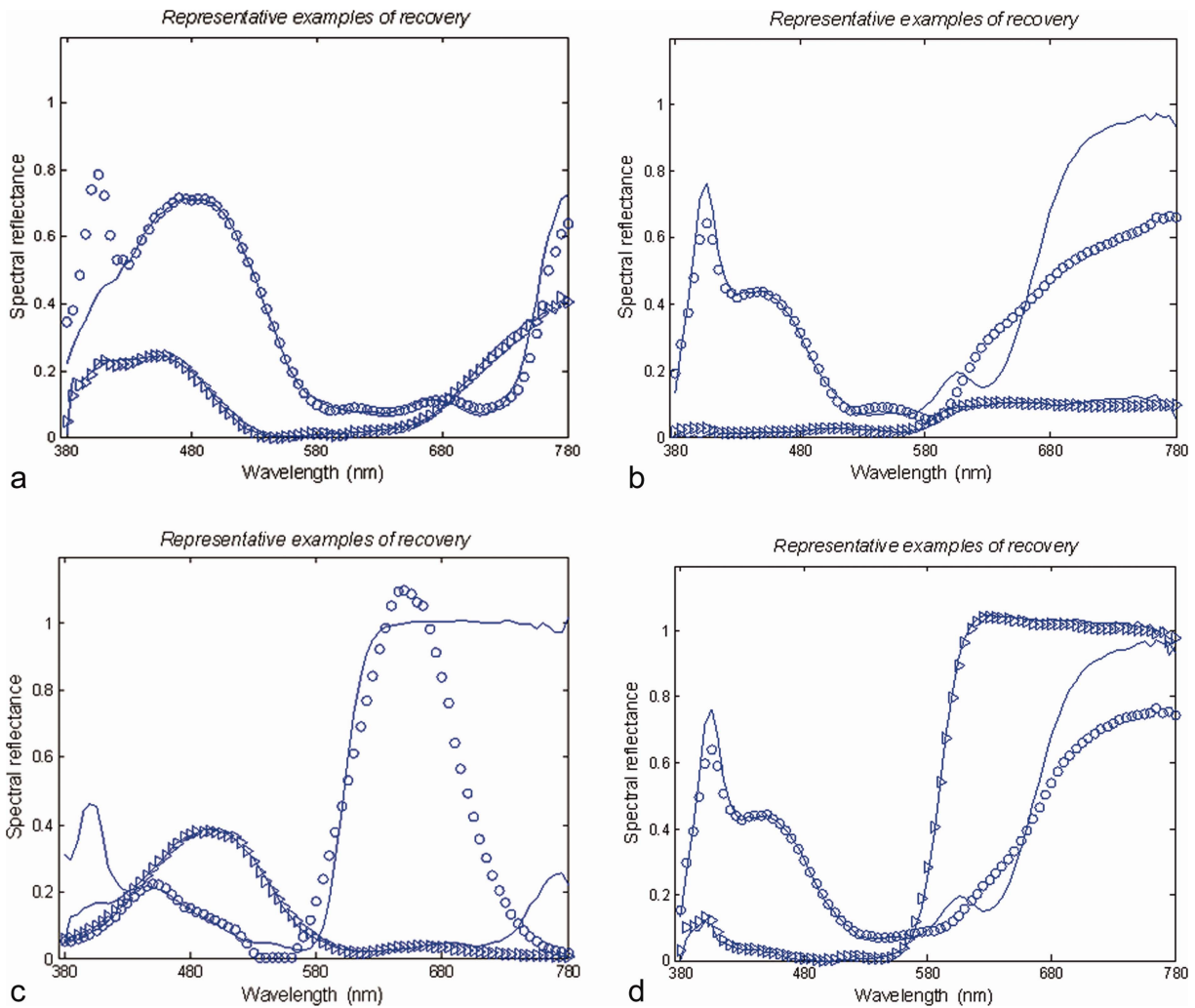


FIG. 3. Representative examples of recovery (corresponding to 5 and 95 percentiles) for sensor set C. (a) RBFNN. (b) Pseudoinverse (c) POCS. (d) kernel. The measured spectra are plotted in continuous lines, and the estimated spectra using symbols. [Color figure can be viewed in the online issue, which is available at [wileyonlinelibrary.com](http://wileyonlinelibrary.com).]

section, we performed the estimations of ink reflectances using sensor set C with reduced spectral range between 430 and 685 nm, and 160 samples of the Color Checker DC (set 2) as well as 160 samples of Vhrel’s reflectances (set 3) for training, instead of using the ink reflectances (set 1). We have found for our data using either alternative training set the best performance is offered by the pseudoinverse algorithm, showing that this algorithm, is most suitable in case a non-optimal training set is used for estimation. Except for the POCS algorithm which does not require training, as outlined in the previous section, all quality indices are worse than those corresponding to estimation based on training set 1. For instance, the best GFC for sensor set C and noisy data decreases from 0.9964 to 0.9924, best RMSE increases from 0.0025 to 0.0040, and the averaged  $\Delta E_{94}$  increases from 1.0352 to 1.7730 for training set 2; the best GFC for training set 3 is 0.9936, best RMSE is 0.0047, and the averaged  $\Delta E_{94}$  is 1.5834. This is not very surprising given the dissimilarities found between the subspaces covered by the different training sets (see “Light Source and Training Samples”

section). Training sets 2 and 3 are constituted by the same number of samples as training set 1, but none of them are printer inks. The two algorithms for which estimation quality decreases most are kernel and RBFNN. This is due to the fundamental principle underlying their estimation process: the RBFNN (as all neural networks) is extremely sensitive to the kind of samples provided in the training phase. The kernel requires tuning of some parameters which depend to a certain degree on the training set as well. Therefore, it is quite logical that RBFNN and kernel are more affected by a relatively bad choice of a training set.

The pseudoinverse algorithm is not influenced as much as RBFNN and kernel by the training set selection. This is a point in favor of this method if an optimized set of training reflectances cannot be found.

#### Sensor Set Optimization by Exhaustive Search

As discussed in “Training Set 1 and Full Spectral Range” section, sensor sets B and C are closer to a real

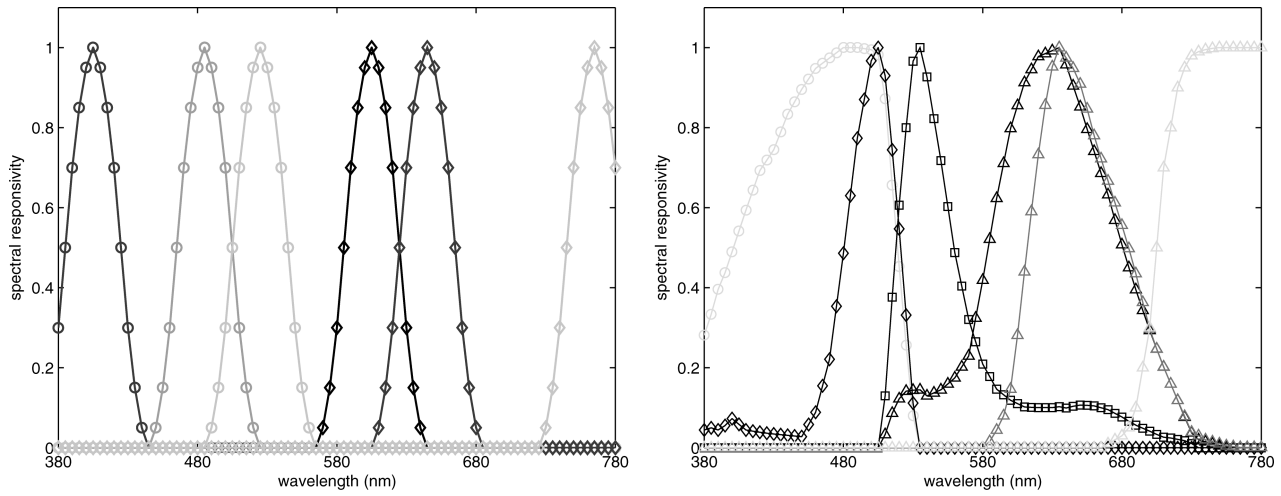


FIG. 4. Optimal six sensors for sensor set A (left) and sensor set B (right). Data based on full spectral range recovery with training set 1 and noisy data.

multispectral system's spectral responsivity, while sensor sets A and B cover the full spectral range of the measurements better. The advantage of sensor set C is the reduced number of sensors when compared with A and B. Both sensor sets A and B have 12 sensors. That number is above the usual number of sensors for multispectral capture devices.<sup>3</sup> Apart from that, it can be seen from Fig. 1 that the sensitivities of the sensors in set B clearly overlap, and the same is true (though to a lesser degree) for sensor set A. We are interested in investigating the possibility of using a reduced number of sensors for these two sensor sets, and to see if we can optimize the sensor selection for spectral estimation in the full spectral range for training set 1. For our study, we used an exhaustive search procedure to determine the optimum sensor subset ranging from six to eight sensors. The computationally expensive exhaustive search process is feasible in our case, because the number of sensors is not very high. Other studies have tackled the issue of sensor or filter set optimization for a specific task,<sup>38–41</sup> and this issue is contemplated as a matter of future work within our specific task of designing a multispectral capture system for in-line inspection of printer inks.

The exhaustive search procedure works in the following way: for each combination of six or eight sensors, we obtain estimated reflectances of sample set 1 for all five algorithms. According to the obtained estimation quality for each algorithm, we assign a rank for the best 10 combinations. These combinations were considered as competitors. Finally, we selected the best combination by taking into account the number of times it appeared in the “best 10” and the given position in the ranking for individual algorithms. So for each combination, if it appeared in “best 10” for each algorithm we added 100 points; and for each time it appeared as the best for a given algorithm, we added 5 points; 4 points were added for each time it appeared as second best, and so on. Finally, we added up all the points for the competitors, and the best combination was selected. The best sensor combination of

six sensors obtained from sets A and B are shown in Fig. 4. Remarkably, in both optimized sensor subsets, there is a higher number of sensors placed in the central portion of the spectral range than in the portions near the extremes of the spectrum. Once again, sensor set A offers the best results, but there is a significant increase in estimation quality for optimized sensor set B as well.

The quality indices for the different algorithms and noisy data for sensor sets A and B and RBFNN algorithm are shown in Table III for six and eight sensors. Adding two more sensors (eight sensors) results in improvement in GFC and  $\Delta E_{94}$  for both sensor sets, and a decrease in GFC for sensor set B while the GFC for sensor set A increases as well. This shows that adding more sensors can sometimes worsen estimation quality, especially for noisy camera sensor responses. We can conclude from this result that it is possible to obtain a high quality recovery with only six real sensors belonging to sensor set B, while for sensor set C it would be necessary to add more sensors in the extremes of the spectrum (and per-

TABLE III. Optimized sensor set quality estimation indices for sensor sets A and B, full spectral range, noisy data, and RBFNN algorithm.

	Set A (6)	Set A (8)	Set B (6)	Set B (8)
		RMSE		
Mean	0.0033	<b>0.0027</b>	<b>0.0036</b>	0.0038
STD	0.0022	0.0018	0.0029	0.0027
5% p	0.001	0.0009	0.0012	0.0014
95% p	0.0066	0.005	0.0062	0.0072
		GFC		
Mean	0.9948	<b>0.9963</b>	<b>0.9936</b>	0.9907
STD	0.0106	0.0073	0.0135	0.0198
5% p	0.9996	0.9996	0.9993	0.9993
95% p	0.9828	0.9876	0.9772	0.9613
		$\Delta E_{94}$		
Mean	1.9727	<b>1.7723</b>	1.6249	<b>1.3543</b>
STD	1.2914	1.5323	0.8158	0.7164
5% p	0.6246	0.5677	0.6202	0.5275
95% p	4.5975	4.0874	2.9439	2.6788

Best results in bold for each metric.

form the exhaustive search optimization) to obtain good quality results for the full spectral range.

If we consider the influence of the algorithm on the estimation results, again the kernel offers the best quality, a result in agreement with findings from previous experiments (see “Training Set 1 and Full Spectral Range” section).

## CONCLUSIONS

We have analyzed the influence of several factors on the performance of a simulated multispectral capture aimed at spectral reflectance estimation of printer inks from sensor responses for in-line color quality inspection of printed samples. Those factors were the estimation algorithm, influence of noise in the camera responses, type of training set, spectral range and selection of an optimal sensor subset. We have found evidence of crossed interactions between some of these factors. The training set selection determines the best estimation algorithm. If the training set is not optimum (i.e., if the samples in the set do not cover the same subspace as the target samples) or if there is no training set available, then POCS or pseudo-inverse algorithms are the best choices. The POCS algorithm does not require a training set and is less sensitive to noise in the sensor responses than pseudoinverse. If an adequate training set can be built, the best results correspond to the kernel algorithm, followed by RBFNN. The spectral range covered by the sensors is a key factor in determining estimation quality. A sensor set covering most of the spectral range of the measurements, and particularly the extremes of the spectrum, should be selected. Nevertheless, the results of exhaustive search selection show that the majority of the optimum sensors would cover the central portion of the spectral range.

Our results pave the way for the implementation of a real multispectral capture system, designed for new applications of spectral estimation related to printer ink reflectances. Apart from that, this study contains some practical advice for capture system designers related to the selection of training samples, optimal sensor sets and evaluation of a suitable spectral estimation algorithm for this specific task.

## ACKNOWLEDGMENTS

The authors thank Mrs. Angela L. Tate for correcting the English in the first version of this article.

- Grahn HF, Geladi P, editors. *Techniques and Applications of Hyperspectral Image Analysis*. Chichester: Wiley; 2007.
- Kerekes JP, Schott JR. Hyperspectral imaging systems, In: Chang CI, editor. *Hyperspectral Data Exploitation: Theory and Applications*. Hoboken NJ: Wiley; 2006.
- Hardeberg JY. *Acquisition and reproduction of color images: colorimetric and multispectral approaches*, Ph.D. Dissertation, Ecole Nationale Supérieure des Télécommunications; 1999.
- Maloney LT, Wandell BA. Color constancy: A method for recovering surface spectral reflectance. *J Opt Soc Am A* 1986;3:29–33.
- Imai FH, Berns RS. Spectral estimation using trichromatic digital cameras, In: *Proceedings of the Internat. Symposium on Multispectral Imaging and Color Reproduction for Digital Archives*. Society of Multispectral Imaging of Japan; 1999, p 42–48.
- Nieves JL, Valero EM, Nascimento SMC, J. Hernández-Andrés, Romero J. Multispectral synthesis of daylight using a commercial digital CCD camera. *Appl Opt* 2005;44:5696–5703.
- Shi M, Healey G. Using reflectance models for color scanner calibration. *J Opt Soc Am A* 2002;19:645–656.
- Pratt WK, Mancill CE. Spectral estimation techniques for the spectral calibration of a color image scanner. *Appl Opt* 1976;15:73–75.
- Zhao Y, Berns RS. Image-based spectral reflectance reconstruction using the matrix R method. *Color Res Appl* 2007;32:343–351.
- Heikkinen V, Lenz R, Jetsu T, Parkkinen J, Hauta-Kasari M, Jääskeläinen T. Evaluation and unification of some methods for estimating reflectance spectra from RGB images. *J Opt Soc Am A* 2008;25:2444–2458.
- Carcagni P, Patria AD, Fontana R, Greco M, Mastroianni M, Materazzi M, Pampaloni E, Pezzati L. Multispectral imaging of paintings by optical scanning. *Opt Laser Eng* 2007;45:360–367.
- Chao K, Yang CC, Chen YR, Kim MS, Chan DE. Hyperspectral-multispectral line-scan imaging system for automated poultry carcass inspection applications for food safety, *Poult Sci*. 2007;86:2450–2460.
- López-Álvarez MA, Hernández-Andrés J, Valero EM, Romero J, Selecting algorithms, sensors and linear bases for optimum spectral recovery of skylight. *J Opt Soc Am A* 2007;24:942–956.
- Bastani B, Funt B. Geodesic based ink separation for spectral printing, In: *Proc. of the 16th Color Imaging Conference, Society for Imaging Science and Technology*. Springfield VA: IS&T, 2008, p 67–72.
- Sharma G, Wang S. Spectrum recovery from colorimetric data for color reproduction, In: *Proc. SPIE, Color Imaging: Device-Independent Color, Color Hardcopy, and Applications VII* 4663. California, USA: San José; 2002, p 8–14.
- Yang Y, Stark H. Solutions of several color matching problems using projection theory. *J Opt Soc Am A* 1994;11:89–96.
- Buhmann MD. *Radial Basis Functions: Theory and Implementations*. Cambridge, UK: Cambridge University Press; 2003.
- Sze SM, *Physics of Semiconductor Devices*, 2nd edition. New York: Wiley; 1981. p 362–510.
- Franco S. *Design with Operational Amplifiers and Analog Integrated Circuits*, 3rd edition. New York, USA: McGraw-Hill; 2002. p 311:346.
- Ratnasingham S, Collins S. Study of the photodetector characteristics of a camera for color constancy in natural scenes. *J Opt Soc Am A* 2010;27:286–294.
- Trussell HJ. Applications of set theoretic methods to color systems. *Color Res Appl* 1991;16:31–41.
- Hu Y, Hernández-Andrés J, Nieves JL, Valero EM, Romero J, Schnitzlein M, Nowack D. Evaluation and optimization of spectral estimation algorithms for printer inks, In: *Proceedings of the AIC 2011 Interim Meeting, Zurich, Switzerland: AIC; 2011. p 422–426*.
- Ribés A, Schmitt F. A fully automatic method for the reconstruction of spectral reflectance curves by using mixture density networks. *Pattern Recog Lett* 2003;24:1691–1701.
- Nieves JL, Valero EM, Plata C, Romero J, Nascimento SMC, Influence of noise in recovering spectral data from natural scenes with an RGB digital camera, In: *Proceedings of the AIC Midterm Meeting, Hangzhou; 2007. p 342–345*.
- Shen HL, Cai PQ, Shao SJ, Xin JH. Reflectance reconstruction for multispectral imaging by adaptive Wiener estimation. *Opt Express* 2007;15:15545–15554.
- Parkkinen J, Hallikainen J, Jaaskelainen T. Characteristic spectra of Munsell colors. *J Opt Soc Am A* 1989;6:318–322.
- Xiong W, Funt B. Independent component analysis and nonnegative linear model analysis of illuminant and reflectance spectra, In: *Proceedings of the Tenth Congress of the International Colour Association*. Granada, Spain: AIC; 2005. p 503–506.
- Nieves JL, Valero EM, Hernández-Andrés J, Romero J. Recovering fluorescent spectra with an RGB digital camera and color filters using different matrix factorizations. *Appl Opt* 2007;46:4144–4154.

29. Akhloufi MA, Bendada A, Batsale JC. Multispectral face recognition using non linear dimensionality reduction, In: Proc. SPIE. Orlando, Florida, USA: Visual Information Processing XVIII, 2009;7341: 73410J.
30. Allen DM. The relationship between variable selection and data augmentation and a method for prediction. *Technometrics* 1974;16: 125–127.
31. Shen HL, Zhang HG, Xin JH, Shao SJ. Optimal selection of representative colors for spectral reflectance reconstruction in a multispectral imaging system. *Appl Opt* 2008;47:2494–2502.
32. Cheung V, Li C, Westland S, Hardeberg JY, Connah DR. Characterization of trichromatic color cameras by using a new multispectral imaging technique. *J Opt Soc Am A* 2005;22:1231–1240.
33. de Lasarte M, Arjona M, Vilaseca M, Pujol J. Influence of the number of samples of the training set on accuracy of color measurement and spectral reconstruction. *J Imaging Sci Technol* 2010;54:030501–030510.
34. Vrhel MJ, Gershon R, Iwan LS. Measurement and analysis of object reflectance spectra. *Color Res Appl* 1994;19:4–9.
35. Romero J, García-Beltrán A, Hernández-Andrés J. Linear bases for representation of natural and artificial illuminants. *J Opt Soc Am A* 1997;14:1007–1014.
36. Viggiano JAS. Metrics for evaluating spectral matches: A quantitative comparison, In: Proceedings of the 2nd European Conference on Colour Graphics, Imaging and Vision. Aachen, Germany: Society for Imaging Science and Technology; 2004. p 286–291.
37. López-Álvarez MA, Hernández-Andrés J, Romero J, Lee RL Jr., Designing a practical system for spectral imaging of skylight. *Appl Opt* 2005;44:5688–5696.
38. Vora P, Trussell HJ. Measure of goodness of a set of color scanning filters. *J Opt Soc Am A* 1993;10:1499–1508.
39. Vrhel MJ, Trussell HJ. Filter considerations in color correction. *IEEE Trans Image Process* 1994;3:147–161.
40. Vora PL, Trussell HJ. Mathematical methods for the design of color scanning filters. *IEEE Trans Image Process* 1997;6:312–320.
41. Haneishi H, Hasegawa T, Hosoi A, Yokoyama Y, Tsumura N, Miyake Y. System design for accurately estimating the spectral reflectance of art paintings. *Appl. Opt.* 2000;39:6621–6632.